

# Caster Car – underactuated ground vehicle with caster wheels

Sebastian KORCZAK 

This paper presents a new type of underactuated ground mobile robot called Caster Car. The platform consists of a front-driven and steered wheel and two uncontrolled rear caster wheels. The Caster Car model presented can be an interesting alternative for mobile robots that connects dynamic properties of hovercrafts and classical 4-wheeled cars. Underactuated properties of the Caster Car cause that classical proportional-derivative feedback control give the ability to affect only selected configuration variables. Three mathematical models of the Caster Car are proposed: a dynamic model with free-moving casters, a dynamic model with blocked casters, and a simplified hovercraft description. Models were tested during tracking tasks with demanding trajectory using selective and full-state control. This full state control was based on the computed torque technique with the pseudoinverse operation and proportional-derivative feedback. It gives the ability to suppress unstable behaviors of uncontrolled orientation but in cost of overall effect (higher position errors).

**Key words:** underactuated system, caster wheel, computed torque technique, pseudoinverse

## 1. Introduction

For years many mobile robot platform types have been developed. Popular three- or four-wheeled platforms often use their kinematic properties for control tasks. Problems related to nonholonomic constraints have been analyzed for years [1, 7] with the success of omnidirectional wheels alternative [17]. Researchers like also more complicated platforms – two-wheeled balancing robots or balancing on a ball robots [14]. Underactuated mechanical systems are one of the most active fields of research related to nonlinear control of flying, driving, and floating objects [12]. Control techniques vary from classical PID, through backstepping and fuzzy approaches [18] to advanced non-holonomic navigators [15].

---

Copyright © 2024. The Author(s). This is an open-access article distributed under the terms of the Creative Commons Attribution-NonCommercial-NoDerivatives License (CC BY-NC-ND 4.0 <https://creativecommons.org/licenses/by-nc-nd/4.0/>), which permits use, distribution, and reproduction in any medium, provided that the article is properly cited, the use is non-commercial, and no modifications or adaptations are made

S. Korczak (e-mail: [sebastian.korczak@pw.edu.pl](mailto:sebastian.korczak@pw.edu.pl)) is with Warsaw University of Technology, ul. Narbutta 84, 02-524 Warsaw, Poland.

Received 13.06.2021. Revised 13.7.2023 and 1.02.2024.

Swivel caster wheels invented by an ancient civilization, patented approximately 100 years ago [2], become a powerful tool for transportation machines and furniture. Typical usage for airplanes was extended for ground vehicles with wheelchair patent [16].

The purpose of this paper is to present a new type of underactuated ground mobile robot called Caster Car. The platform consists of a front-driven and steered wheel, and two rear caster wheels (Figure 1). These passive caster wheels adapt their orientation to the platform's velocity direction. The behavior of the platform is similar to a hovercraft but the caster wheels' friction extends it with some new types of motion with uncertainty of the center of rotation's location. This system with three degrees of freedom and two inputs is formally called trivially underactuated. Underactuation property limits the range of system accelerations, even with unbounded inputs [6]. As presented in [11] this type of underactuated system is vulnerable to chaotic behaviors in case of trajectory tracking with limited direction of input force.

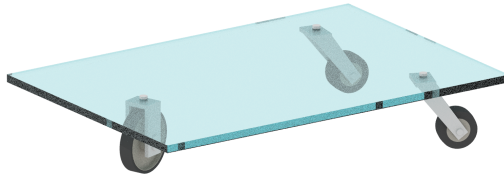


Figure 1: Caster Car

Traditional vehicles have front-driven and rotating wheels and rear fixed-axis wheels. This causes a limitation of the minimum value of the radius of trajectory curvature when assuming motion without a slip (classical first-order nonholonomic constraints). Second-order nonholonomic constraints (underactuation) limit accelerations without the limitation of velocities directions, thus control of the Caster Car becomes more flexible and challenging.

## 2. Caster Car overview

Caster Car presented in Figure 1 consists of a chassis with two rear caster wheels and one front-driven and steered wheel (alternatively two front wheels are possible to prevent overturning). In the case of rolling without a slip, a front-driven wheel and rear passive wheels of the Caster Car are oriented to satisfy the instantaneous velocity scheme of a chassis. Possible types of steady motion of the system are shown in Figure 2:

- a) linear motion in a direction parallel to the platform's longitudinal axis of symmetry,

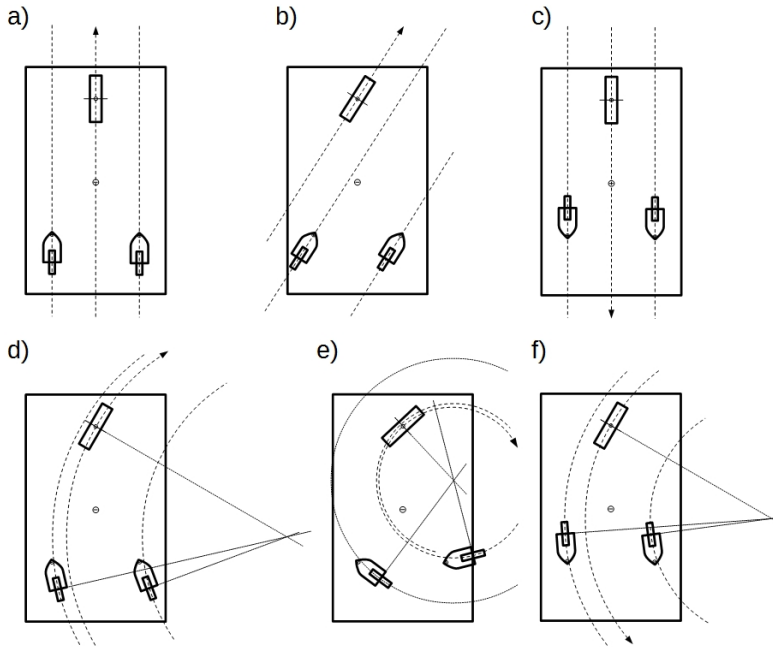


Figure 2: Possible steady motions of the Caster Car

- b) skew linear motion – possible due to torque of friction presence in caster wheel pivot,
- c) backward linear motion,
- d) circular motion with a relatively large radius of curvature,
- e) circular motion with a relatively small radius of curvature,
- f) backward circular motion – possible with a relatively small or large radius of curvature.

Dry friction presence in caster wheel pivots causes uncertainty in system’s dynamic behavior. The temporary position of a center of rotation is not directly related to a steering angle of the front wheel, but also depends on a ‘history of motion’. It has been noticed during experiments that underactuated behaviors of the Caster Car moving backward are not as strong as in forward motion (pushing force causes torque on the caster in the same direction as intended by a steered wheel).

Complicated dynamical behaviors of the Caster Car could be mastered or reduced with some construction modifications (not analyzed here):

- a) brakes for the casters – used to keep casters’ direction fixed or to increase friction,

- b) torsional springs for the casters – generates an additional forces attracting to a certain caster position, therefore they reduce variation of casters' directions,
- c) cam follower mechanism – generates centering torque, patented [3,4].

### 3. Mathematical modeling of the Caster Car

#### 3.1. Hovercraft model

The simplest method to describe the dynamics of the Caster Car is to use hovercraft mathematical model. The model described by [9] consist of a planar rigid body moving on a plane (Figure 3). The object has mass  $m$  and inertia  $I_C$  respect to the center of mass (point  $C$ ). Its configuration is described by  $x(t)$  and  $y(t)$  position coordinates and angle  $\varphi(t)$  between the object symmetry line and  $X$  axis of the global coordinate system  $O_{XY}$ . The vector of force  $\vec{F}$  acts on the object in a point away from the center of mass by distance  $a$  and angle  $\beta$ . Constant drag coefficients  $c$  and  $c_\varphi$  are used for linear and angular motion, respectively. The system's equations of motion are as follows

$$m\ddot{x}(t) + c\dot{x}(t) = |\vec{F}(t)| \cos(\varphi(t) + \beta(t)), \quad (1)$$

$$m\ddot{y}(t) + c\dot{y}(t) = |\vec{F}(t)| \sin(\varphi(t) + \beta(t)), \quad (2)$$

$$I_c\ddot{\varphi}(t) + c_\varphi\dot{\varphi}(t) = a|\vec{F}(t)| \sin(\beta(t)). \quad (3)$$

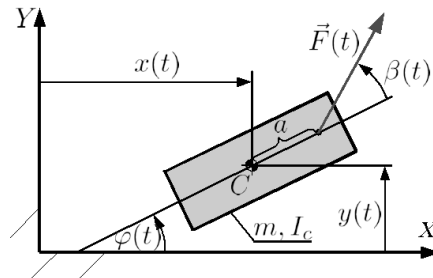


Figure 3: Hovercraft model scheme

The presented model was successfully used to control hovercrafts, rockets, and ships in trajectory tracking tasks. The computed torque technique, backstepping algorithm, passive velocity field method, and sliding mode control have been used in selective control tracking tasks. Many control problems are related to the input coupling effect visible in equations (1)–(3) – both inputs,  $\vec{F}(t)$  and  $\beta(t)$ , presents in more than one equation. The new method of full configuration control with pseudoinverse operation was presented in [10].

### 3.2. Advanced model

The second proposed method of the Caster Car dynamic description is based on the geometry scheme presented in Figure 4, forces/torques description presented in Figure 5 and equations as follows

$$m\ddot{x} = T_t \cos(\varphi + \beta) - T_n \sin(\varphi + \beta) + T_{12x} - c\dot{x}, \quad (4)$$

$$m\ddot{y} = T_t \sin(\varphi + \beta) + T_n \cos(\varphi + \beta) + T_{12y} - c\dot{y}, \quad (5)$$

$$I_C\ddot{\varphi} = a(T_t \sin\beta + T_n \cos\beta) - c_\varphi\dot{\varphi} + M_{1\varphi} + M_{2\varphi}, \quad (6)$$

$$I_F\ddot{\alpha} = M_{Fn} - T_t r_F - c_\alpha\dot{\alpha}, \quad (7)$$

$$I_t(\ddot{\gamma}_1 + \ddot{\varphi}) = -M_1 - T_{1n}e_t, \quad (8)$$

$$I_t(\ddot{\gamma}_2 + \ddot{\varphi}) = -M_2 - T_{2n}e_t, \quad (9)$$

where the car chassis is represented by a rigid body with the center of mass in point  $C$ , parameters and variables  $m$ ,  $I_C$ ,  $x$ ,  $y$ ,  $\varphi$ ,  $c$ ,  $c_\varphi$  defined as in hovercraft model. A front wheel of radius  $r_F$  and inertia described by  $I_F$ , forced by a torque  $M_{Fn}$ , located at distance  $a$  from the center of mass, is rotating with angular velocity  $\omega = \frac{d\alpha}{dt}$  (where  $\alpha$  is the wheel's self-rotation angle). The front wheel's direction angle  $\beta$  also points out the orientation of its local coordinate system  $X_k Y_k$ . Angles  $\gamma_1$  and  $\gamma_2$  are the orientations of the left and right caster wheels'

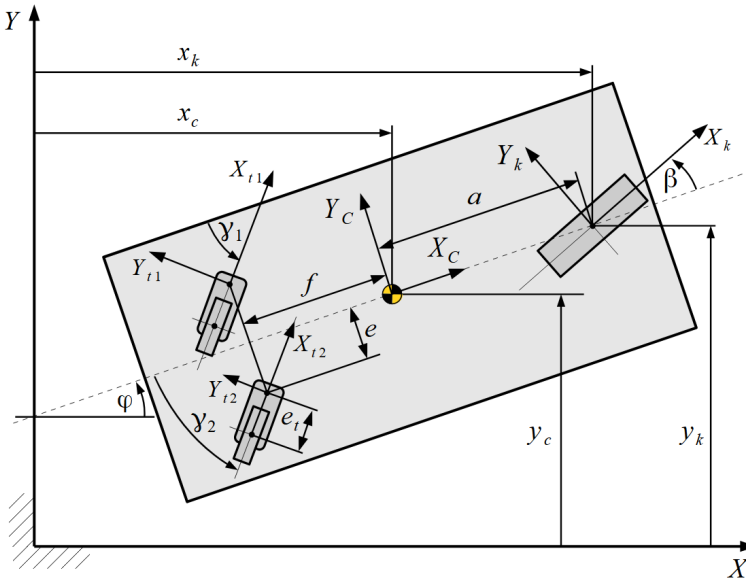


Figure 4: Advanced Caster Car model scheme



$T_{1n} = Q_C \mu_4 \text{sgn}(v_{Cn1})$ ,  $T_{2n} = Q_C \mu_4 \text{sgn}(v_{Cn2})$ ,  $T_{1t} = Q_C \mu_5 \text{sgn}(v_{Ct1})$  and  $T_{2t} = Q_C \mu_5 \text{sgn}(v_{Ct2})$  are lateral friction forces and tangential rolling resistance forces between caster wheels and the ground, but this contact point lay away from a caster kingpin at distance  $e_t$  (caster offset).  $Q_C$  is caster wheel's load,  $\mu_4$  is a dry friction coefficient,  $\mu_5$  is a rolling resistance coefficient,  $v_{Ct1}$ ,  $v_{Ct2}$ ,  $v_{Cn1}$  and  $v_{Cn2}$  are wheel's velocities in contact points (longitudinal and lateral respectively).  $M_1 = Q_C \mu_6 \text{sgn}(\dot{\gamma}_1) + c_7 \dot{\gamma}_1$  and  $M_2 = Q_C \mu_6 \text{sgn}(\dot{\gamma}_2) + c_7 \dot{\gamma}_2$  are dry+viscous friction torques in the caster pivots with constant coefficients  $\mu_6$  and  $c_7$ .

The presented mathematical model has six degrees of freedom – its configuration is described by a set of values  $[x(t), y(t), \varphi(t), \alpha(t), \gamma_1(t), \gamma_2(t)]$  and just two inputs:  $\beta(t)$  and  $M_{Fn}(t)$ . Thus system is trivially underactuated, but inputs are coupled.

#### 4. Dynamic behaviors of the Caster Car

##### 4.1. Parameters of the mathematical models

In this section, exemplary behaviors will be compared for three models:

- A) the Caster Car with blocked casters' yokes (advanced model used),
- B) the Caster Car with freely moving casters (advanced model used),
- C) hovercraft model.

Parameters of the mathematical model are presented in Table 1 and were chosen as follows:

- a) mass and geometrical properties refer to a real experimental mobile platform – a simple plastic plane with solid-rubber wheels with ball bearings, driven by a DC motor with a servomotor and controlled over Bluetooth, mass moment of inertia measured with a torsional pendulum,
- b) front wheel's longitudinal friction force parameters (Burckhardt model –  $\mu_1, \mu_2, \mu_3$ ) were chosen to approximate the standard tire/road adhesion coefficient graph [13],
- c) front wheel's lateral dry friction coefficient parameter  $\mu_4$  was arbitrarily chosen high to model a hard rubber wheel operating with very small side slip angles,
- d) caster wheels' dry friction (lateral component) parameter  $\mu_4$  was arbitrarily chosen to model hard rubber/ground contact,
- e) caster wheels' dry friction (longitudinal component) parameter  $\mu_5$  was assumed to model only small rolling resistance (caster wheel self-rotation omitted),

- f) Coulomb's dry friction torque in caster pivot – parameter  $\mu_6$  was chosen to stabilize numerical simulation,
- g) viscous friction torque in caster pivot coefficient  $c_7$  was chosen to observe good behavior during real-time simulation,
- h) main chassis viscous damping in linear motion  $c$  was identified by speed-up and slow-down experiments (comparison of velocity charts),
- i) angular motion damping  $c_\varphi$  was assumed to stabilize angular motion.

One can notice that for the hovercraft model, the magnitude of input force  $\vec{F}(t)$  is limited and also its directing angle  $\beta(t)$  is limited to the symmetric region. This cause only forward motion to be possible.

Table 1: Parameters of the mathematical model used to simulate the Caster Car behavior

Common parameters for all models
$m = 1.7 \text{ kg}$ , $I_C = 0.003 \text{ kg}\cdot\text{m}^2$ , $a = 89 \text{ mm}$ , $c = 0.6 \text{ N}\cdot\text{s}\cdot\text{m}^{-1}$ , $c_\varphi = 0.01 \text{ N}\cdot\text{m}\cdot\text{s}$ , $c_\alpha = 0.001 \text{ N}\cdot\text{m}\cdot\text{s}$ , $\beta(t) \in [-60^\circ, 60^\circ]$
Parameters for the Caster Car model
$f = 110 \text{ mm}$ , $e = 64.5 \text{ mm}$ , $e_t = 18.5 \text{ mm}$ , $r_F = 25.8 \text{ mm}$ , $I_F = 10^{-7} \text{ kg}\cdot\text{m}^2$ , $I_T = 10^{-7} \text{ kg}\cdot\text{m}^2$ , $\mu_1 = \mu_4 = 1.1$ , $\mu_2 = 20$ , $\mu_3 = 0.2$ , $\mu_5 = 10^{-3}$ , $\mu_6 = 5 \cdot 10^{-5} \text{ m}$ , $c_7 = 10^{-6} \text{ N}\cdot\text{m}\cdot\text{s}/\text{rad}$ , $M_{Fn} = 0.03 \text{ N}\cdot\text{m}$
Parameter for the Hovercraft model
$ \vec{F}(t)  \leq 1.2 \text{ N}$

#### 4.2. Motion range maps

With numerical simulations, regions of possible model positions were described for analyzed models with arbitrarily chosen time periods and zero initial conditions (Figure 6). The motion range map for the Caster Car with blocked casters' yokes (A) is limited by the first-order nonholonomic constraints with steering angle saturation (Figure 6a). The corresponding map for the Caster Car with freely moving casters' yokes (B) comes from its underactuated properties – second-order nonholonomic constraints (Figure 6b). The motion range map for the hovercraft model (C) is limited by the steering angle saturation, system's inertia, and environment viscosity according to its underactuated properties (Figure 6c). All maps are limited by the motion time in relation to the maximum available force and model mass.

The region of possible positions of the Caster Car with freely moving yokes is different than in the corresponding model with blocked yokes – some new regions

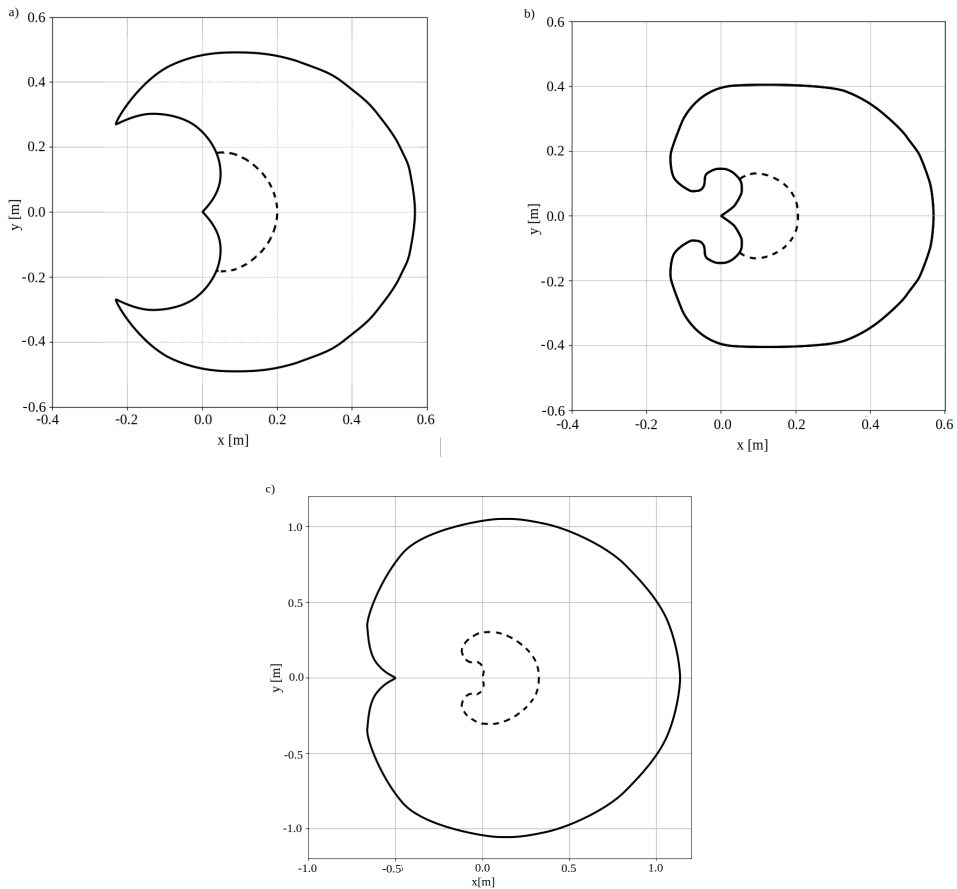


Figure 6: Regions of possible model position with motion limited to 1 s (dashed line) and 2 s (continuous line): a) Caster Car with blocked casters' yokes, b) Caster Car with freely moving casters' yokes, c) hovercraft model

of configuration are accessible. That gives possibility to extend the agility of a classical nonholonomic 4-wheels mobile platforms by expanding them with caster wheels. The most extensive motion range for the hovercraft model comes from its purely inertial behavior without friction to the ground. The lack of friction related to caster wheels for the hovercraft model caused its higher range with respect to the Caster Car model.

### 5. Control of the Caster Car

In this section, exemplary tracking task for the Caster Car will be presented. Achieved trajectories will be compared for three models: A, B, and C. Parameters

of the mathematical model stay unchanged. The trajectory (Figure 7) consist of 14 parts (lines, arcs, eight-shape, point). This parametric trajectory is described with two constants:  $v_0$  and  $l_0$  as shown in Table 2, where  $x_d(t)$  and  $y_d(t)$  describe position in Cartesian coordinate system and  $\varphi_d(t)$  describes orientation tangential

Table 2: Parametric description of the desired trajectory. Time is described separately for each part

part	$t \in$	$x_d(t)$	$y_d(t)$	$\varphi_d(t)$
1	$\left\langle 0, 8 \frac{l_0}{v_0} \right\rangle$	$v_0 t$	0	0
2	$\left\langle 0, 6\pi \frac{l_0}{v_0} \right\rangle$	$8l_0 + 2l_0 \sin\left(\frac{v_0 t}{2l_0}\right)$	$2l_0 - 2l_0 \cos\left(\frac{v_0 t}{2l_0}\right)$	$\frac{v_0}{2l_0} t$
3	$\left\langle 0, 7 \frac{l_0}{v_0} \right\rangle$	$8l_0 - t v_0$	$4l_0$	$3\pi$
4	$\left\langle 0, \pi \frac{l_0}{v_0} \right\rangle$	$l_0 - l_0 \sin\left(\frac{v_0 t}{l_0}\right)$	$5l_0 - l_0 \cos\left(\frac{v_0 t}{l_0}\right)$	$3\pi - \frac{v_0}{l_0} t$
5	$\left\langle 0, \frac{l_0}{v_0} \right\rangle$	$l_0 + t v_0$	$6l_0$	$2\pi$
6	$\left\langle 0, 5 \frac{l_0}{v_0} \right\rangle$	$2l_0$	$6l_0 + t v_0$	$2.5\pi$
7	$\left\langle 0, 3 \frac{l_0}{v_0} \right\rangle$	$2l_0$	$11l_0 - t v_0$	$1.5\pi$
8	$\left\langle 0, 2 \frac{l_0}{v_0} \right\rangle$	$2l_0 + t v_0$	$8l_0$	$2\pi$
9	$\left\langle 0, 2 \frac{l_0}{v_0} \right\rangle$	$4l_0$	$8l_0 - t v_0$	$1.5\pi$
10	$\left\langle 0, 2 \frac{l_0}{v_0} \right\rangle$	$4l_0 + t v_0$	$6l_0$	$2\pi$
11	$\left\langle 0, 2 \frac{l_0}{v_0} \right\rangle$	$6l_0 + t v_0$	$6l_0 + t v_0$	$2.25\pi$
12	$\left\langle 0, 8\pi \frac{l_0}{v_0} \right\rangle$	$8l_0 + l_0 \sin\left(\frac{v_0 t}{l_0}\right)$	$8l_0 + 2l_0 \sin\left(\frac{v_0 t}{2l_0}\right)$	$3\pi - 2.26 \cos\left(\frac{v_0}{2l_0} t\right)$ $-0.24 \cos\left(\frac{3v_0}{2l_0} t\right)$ $+0.16 \cos\left(\frac{5v_0}{2l_0} t\right)$
13	$\left\langle 0, 3 \frac{l_0}{v_0} \right\rangle$	$8l_0 + t v_0$	$8l_0$	$2\pi$
14	$\left\langle 0, 5 \frac{l_0}{v_0} \right\rangle$	$11l_0$	$8l_0$	$2\pi$

to the trajectory. Simulations for all models were made with trajectory parameters  $v_0 = 0.2 \text{ m}\cdot\text{s}^{-1}$  and  $l_0 = 0.2 \text{ m}$ .

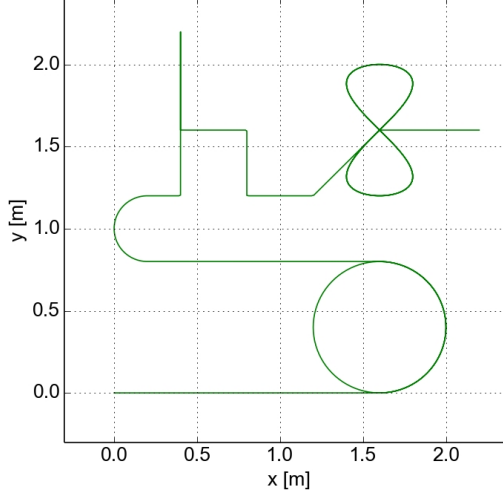


Figure 7: Desired trajectory for  $l_0 = 0.2 \text{ m}$

### 5.1. Selective control with PD controller

The center of mass position of the Caster Car model could be controlled with classical proportional-derivative feedback. Let's define tracking problem with a desired planar trajectory described by position functions  $x_d(t)$  and  $y_d(t)$ . Control errors are then defined as  $e_x(t) = x_d(t) - x(t)$  and  $e_y(t) = y_d(t) - y(t)$ . Basic control functions are then as follows

$$\tau_x(t) = k_D (\dot{x}_d(t) - \dot{x}(t)) + k_P (x_d(t) - x(t)), \quad (14)$$

$$\tau_y(t) = k_D (\dot{y}_d(t) - \dot{y}(t)) + k_P (y_d(t) - y(t)). \quad (15)$$

For the hovercraft model, it gives inputs

$$F(t) = \sqrt{\tau_x^2 + \tau_y^2}, \quad (16)$$

$$\beta(t) = \text{Arg}(\tau_x + \tau_y \sqrt{-1}) - \varphi(t). \quad (17)$$

For the Caster Car model the front wheel's direction angle  $\beta(t)$  should be controlled with function (17) and front wheel's torque should be calculated with relation to (16)

$$M_{Fn}(t) = F(t)r_F. \quad (18)$$

## 5.2. Full state control with computed torque technique and pseudoinverse

Position and rotation of the Caster Car model could be controlled using full state control method based on the computed torque technique with the pseudoinverse operation and proportional-derivative feedback presented in [9]. Let's define the tracking problem of desired trajectory described by  $x_d(t)$  and  $y_d(t)$ , with desired tangential orientation  $\varphi_d(t)$  with respect to trajectory. Control errors are then defined as

$$\mathbf{e}(t) = \mathbf{d}(t) - \mathbf{q}(t), \quad (19)$$

where

$$\mathbf{d} = [x_d(t) \ y_d(t) \ \varphi_d(t)]^T, \quad (20)$$

$$\mathbf{q} = [x(t) \ y(t) \ \varphi(t)]^T. \quad (21)$$

Hovercraft equations (1)–(3) could be described in matrix form

$$\ddot{\mathbf{q}}(t) = \mathbf{f}_1 + \mathbf{f}_2 \mathbf{u}(t), \quad (22)$$

where

$$\mathbf{f}_1 = \begin{bmatrix} -\frac{c}{m} \dot{x}(t) \\ -\frac{c}{m} \dot{y}(t) \\ -\frac{c_\varphi}{I_C} \dot{\varphi}(t) \end{bmatrix}, \quad (23)$$

$$\mathbf{f}_2 = \begin{bmatrix} \frac{\sin \varphi(t)}{m} & \frac{\cos \varphi(t)}{m} \\ \frac{\cos \varphi(t)}{m} & \frac{\sin \varphi(t)}{m} \\ \frac{a}{I_C} & 0 \end{bmatrix}, \quad (24)$$

$$\mathbf{u} = \begin{bmatrix} f(t) \sin \beta(t) \\ f(t) \cos \beta(t) \end{bmatrix}. \quad (25)$$

Advanced Caster Car model can be described in the form of equation (22) with components

$$f_1 = \begin{bmatrix} (T_{12x} - c\dot{x}(t))/m \\ (T_{12y} - c\dot{y}(t))/m \\ (M_{1\varphi} + M_{2\varphi} - c_\varphi\dot{\varphi}(t))/I_c \\ -(T_t r_F + c_\alpha\dot{\alpha})/I_F \\ (T_{1n}e_t - M_1)/I_t + \ddot{\varphi} \\ (T_{2n}e_t - M_2)/I_t + \ddot{\varphi} \end{bmatrix} \quad (26)$$

$$f_2 = \begin{bmatrix} f_{2(11)} & f_{2(12)} & 0 & 0 \\ f_{2(21)} & f_{2(22)} & 0 & 0 \\ aT_t/I_C & aT_n/I_C & 0 & 0 \\ 0 & 0 & 0 & 1/I_F \\ 0 & 0 & 0 & 0 \\ 0 & 0 & 0 & 0 \end{bmatrix}, \quad (27)$$

$$u = \begin{bmatrix} \sin \beta(t) \\ \cos \beta(t) \\ 0 \\ M_{Fn}(t) \end{bmatrix}, \quad (28)$$

where

$$f_{2(11)} = -(T_t \sin \varphi(t) + T_n \cos \varphi(t)) / m, \quad (29)$$

$$f_{2(12)} = (T_t \cos \varphi(t) - T_n \sin \varphi(t)) / m, \quad (30)$$

$$f_{2(21)} = (T_t \cos \varphi(t) + T_n \sin \varphi(t)) / m, \quad (31)$$

$$f_{2(22)} = (T_t \sin \varphi(t) - T_n \cos \varphi(t)) / m, \quad (32)$$

and configuration matrix defined as

$$q = [x(t) \ y(t) \ \varphi(t) \ \alpha(t) \ \gamma_1(t) \ \gamma_2(t)]^T. \quad (33)$$

Usage of this representation for the computed torque method is impossible because of indirect relation between input torque  $M_{Fn}$  and friction force  $T_t$  (desired wheel's rotation function  $\alpha(t)$  can't be proposed). Assuming friction force  $T_t$  much greater than  $T_n$ , neglecting  $T_{12x}$ ,  $T_{12y}$ ,  $M_{1\varphi}$  and  $M_{2\varphi}$ , gives the possibility to approximate the Advanced Caster Car model with the hovercraft one.

Control functions from computed torque technique with PD feedback are proposed as

$$\begin{bmatrix} \tau_x \\ \tau_y \end{bmatrix} = \mathbf{f}_2^+ (\ddot{\mathbf{d}}(t) - \mathbf{f}_1 + \mathbf{K}_D \dot{\mathbf{e}}(t) + \mathbf{K}_P \mathbf{e}(t)), \quad (34)$$

where  $\mathbf{K}_P = \text{diag}(k_P, k_P, k_{rP})$  and  $\mathbf{K}_D = \text{diag}(k_D, k_D, k_{rD})$  are diagonal matrices of positive coefficients,  $\mathbf{f}_2^+$  is a Moore-Penrose pseudoinverse of  $\mathbf{f}_2$ , that can be calculated with formula [5]

$$\mathbf{f}_2^+ = \lim_{\delta \rightarrow 0} (\mathbf{f}_2^T \mathbf{f}_2 - \delta \mathbf{I})^{-1} \mathbf{f}_2^T. \quad (35)$$

Hovercraft model representation (equation (22)) was used to fill the computed torque part of control functions in the equation (34). Control functions (34) then should be substituted into (16)–(18) for both models' input calculations.

### 5.3. Numerical simulations

For presented three models of the Caster Car (A, B, and C), trajectory tracking task was simulated for the proposed test trajectory and two control techniques. For selective control method  $k_P$  and  $k_D$  parameters were chosen to find the minimum sum of squares of position tracking errors, separately for models A, B, and C. Full state control for all models was prepared to find the minimum sum of squares of position and rotation tracking errors by tuning  $k_P$ ,  $k_D$ ,  $k_{rP}$  and  $k_{rD}$  parameters. Simulations were performed with zero initial conditions except  $y(t=0) = 0.1$  m.

Figures 8–9 presents simulation results of selective and full state control for the Caster Car model with blocked casters (A). Position control presents very good results of trajectory tracking with only one intense deviation from trajectory during 180 deg returning (Figure 8a). Full state control algorithm keeps position and rotation stable during whole motion, reducing deviation of angle errors in cost of position errors (Fig. 9b).

Figures 10–11 presents simulation results of selective and full state control for the Caster Car model with freely moving casters (B). Position control presents very good results of trajectory tracking with only small deviations from trajectory around 180 deg returning (Figure 10a). Full state control algorithm keeps position and rotation stable during whole motion, reducing deviation of angle errors in cost of position errors (Figure 11b).

Figures 14–15 presents simulation results of selective and full state control for the hovercraft model (C). Position control presents good results of trajectory tracking with visible deviations from trajectory starting from the first 90 deg turning point around 38 second (Figure 14a). Full state control algorithm keeps

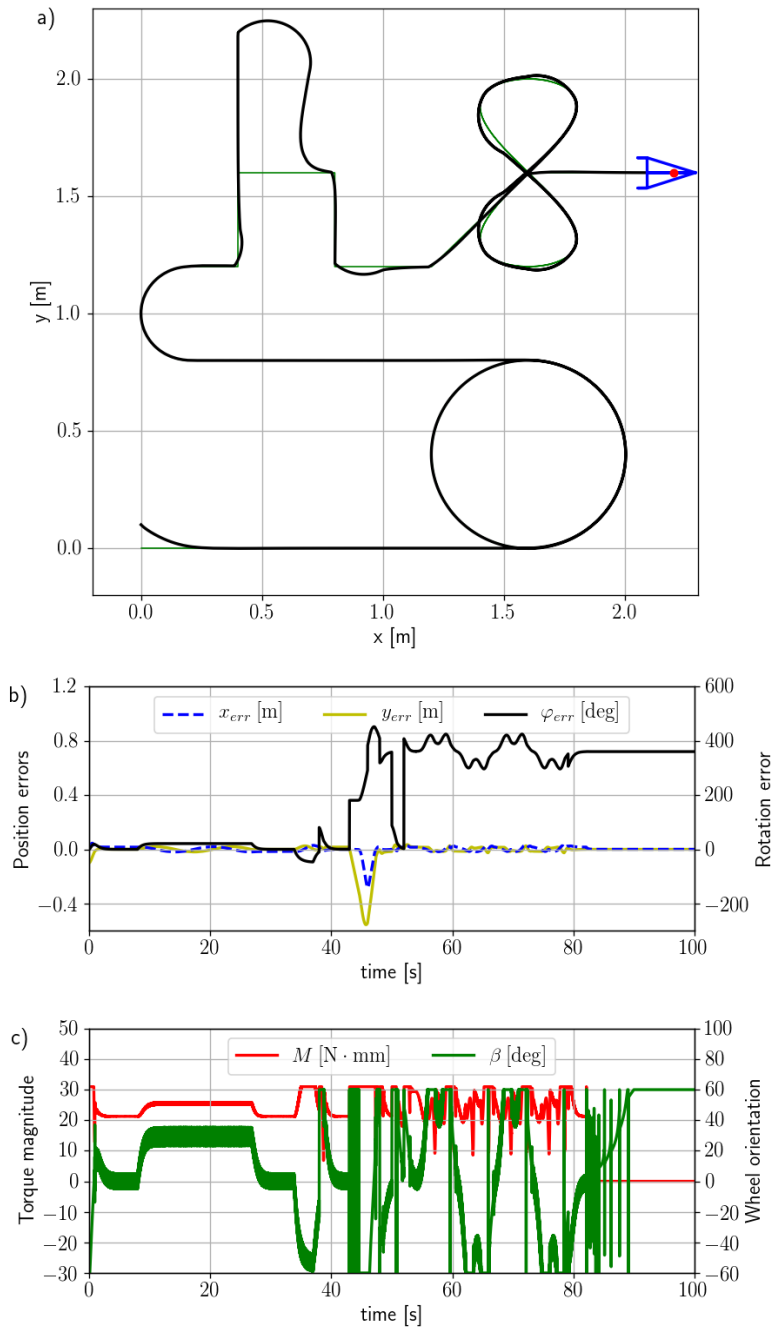


Figure 8: Simulation results of selective control for the Caster Car model with blocked casters (A) and  $k_P = 50.635$ ,  $k_D = 10.004$ : a) desired (green) and achieved (black) trajectories, b) position and rotation errors, c) control signals

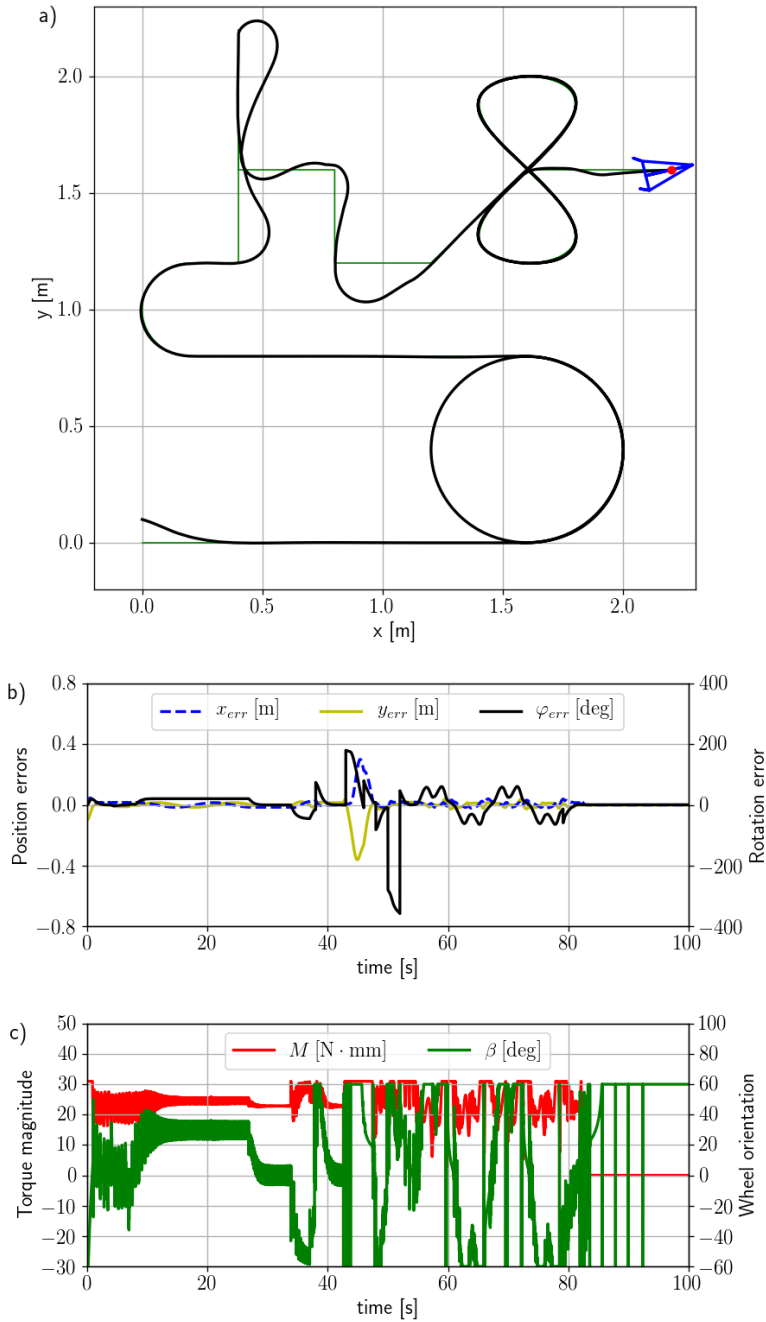


Figure 9: Simulation results of full state control for the Caster Car model with blocked casters (A) and  $k_P = 50.686$ ,  $k_D = 4.964$ ,  $k_{rP} = 4.972$ ,  $k_{rD} = 4.572$ : a) desired (green) and achieved (black) trajectories, b) position and rotation errors, c) control signals

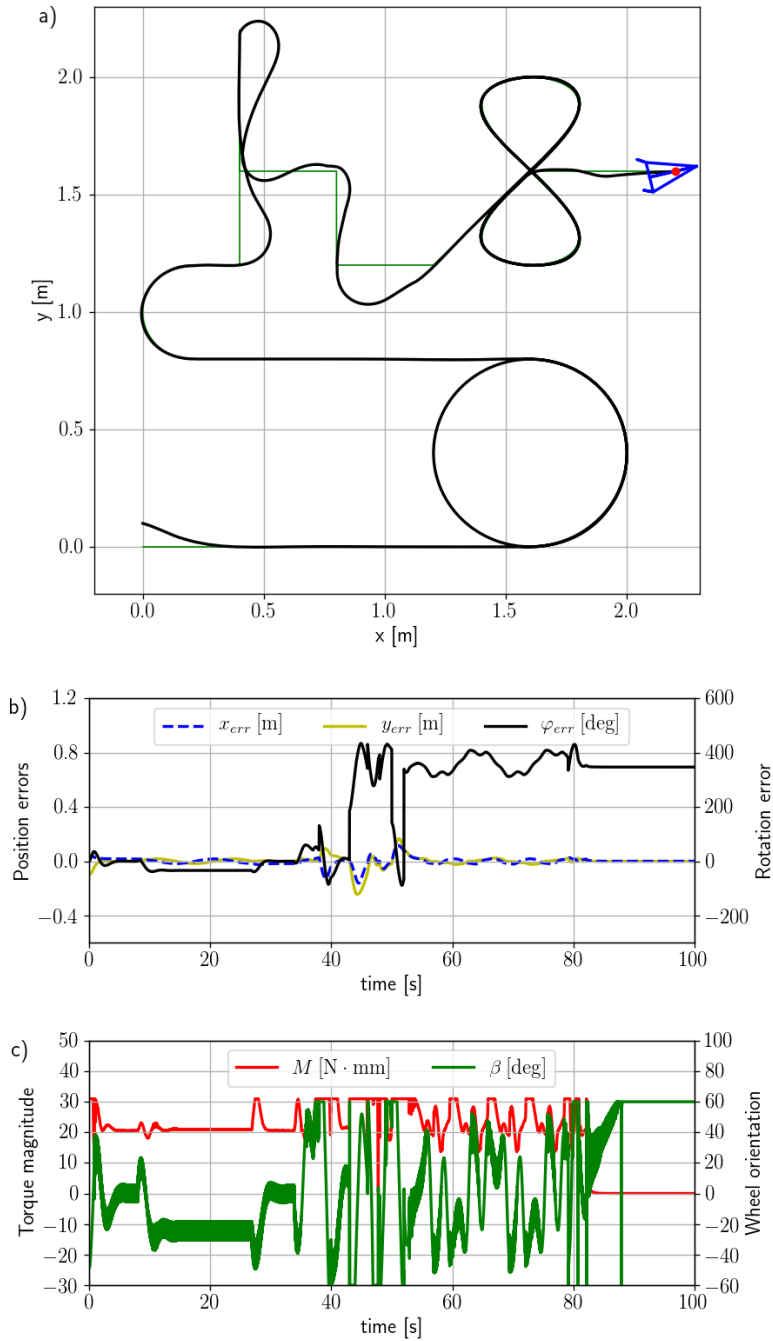


Figure 10: Simulation results of selective control for the Caster Car model with freely moving casters (B) and  $k_P = 45.617$ ,  $k_D = 20.402$ : a) desired (green) and achieved (black) trajectories, b) position and rotation errors, c) control signals

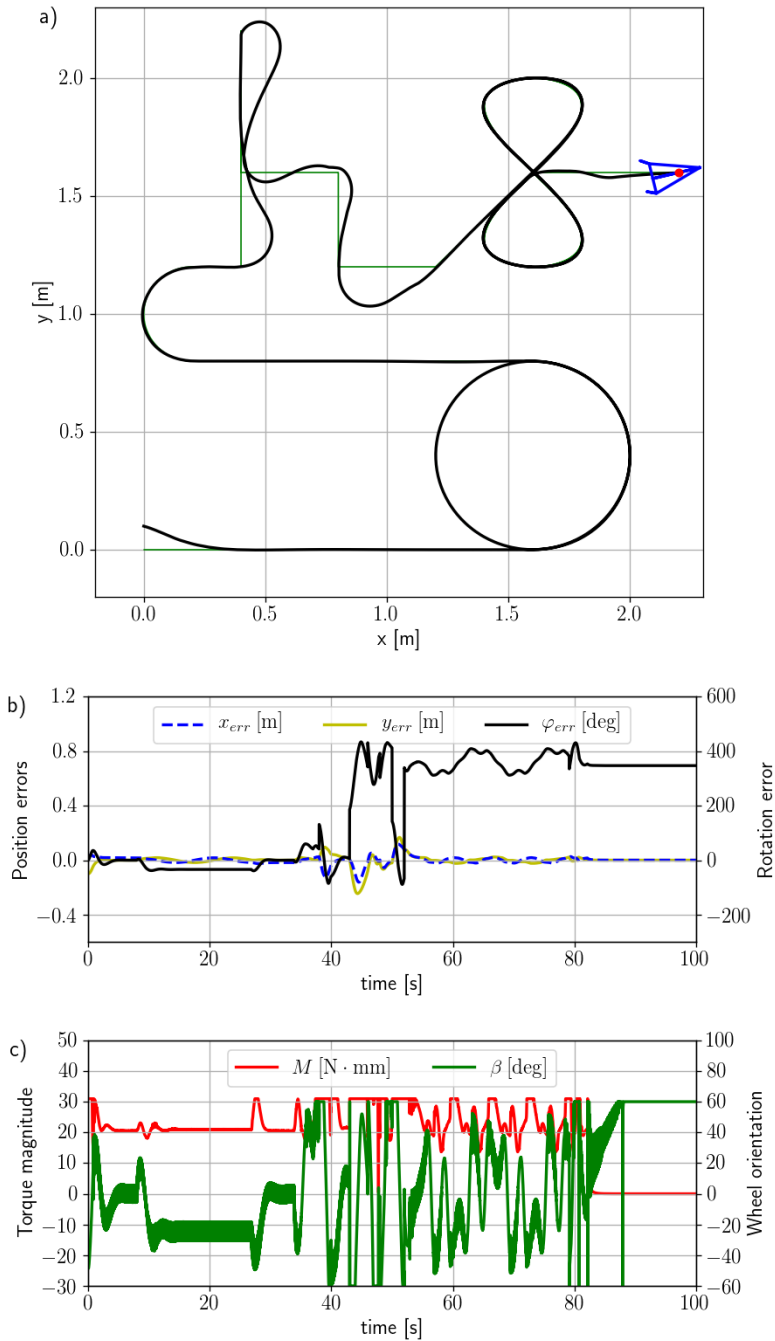


Figure 11: Simulation results of full state control for the Caster Car model with freely moving casters (B) and  $k_P = 5.007$ ,  $k_D = 5.148$ ,  $k_{rP} = 4.861$ ,  $k_{rD} = 4.924$ : a) desired (green) and achieved (black) trajectories, b) position and rotation errors, c) control signals

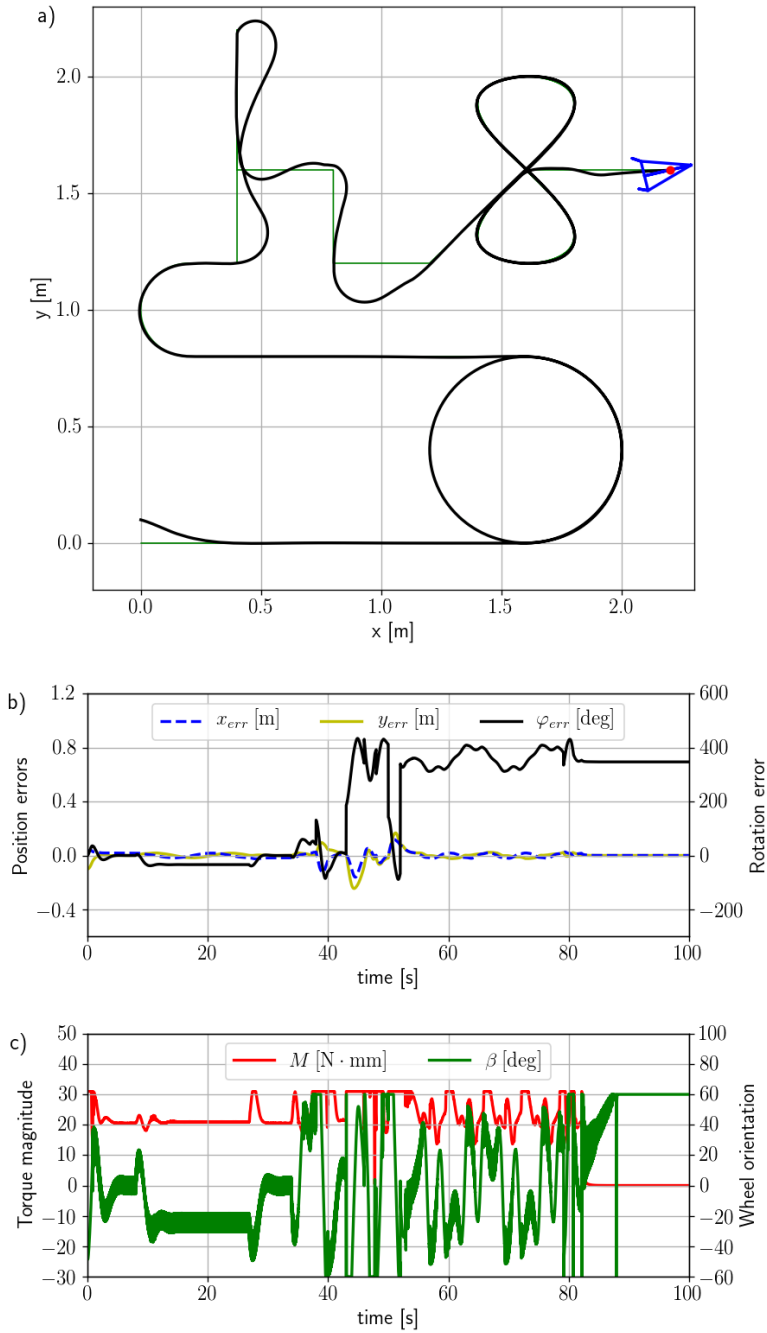


Figure 12: Simulation results of selective control for the Caster Car model with freely moving casters (B) and  $k_P = 45.617$ ,  $k_D = 20.402$ : a) desired (green) and achieved (black) trajectories, b) position and rotation errors, c) control signals

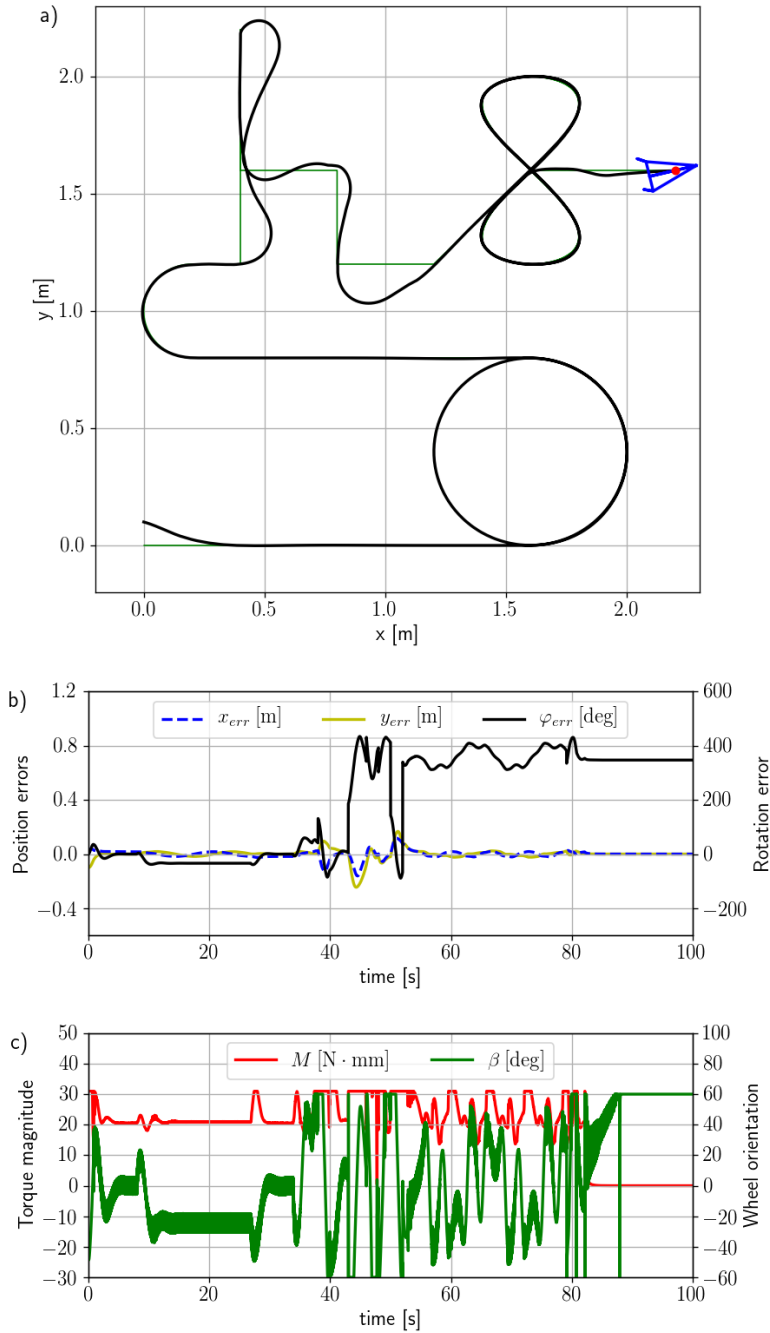


Figure 13: Simulation results of full state control for the Caster Car model with freely moving casters (B) and  $k_P = 5.007$ ,  $k_D = 5.148$ ,  $k_{rP} = 4.861$ ,  $k_{rD} = 4.924$ : a) desired (green) and achieved (black) trajectories, b) position and rotation errors, c) control signals

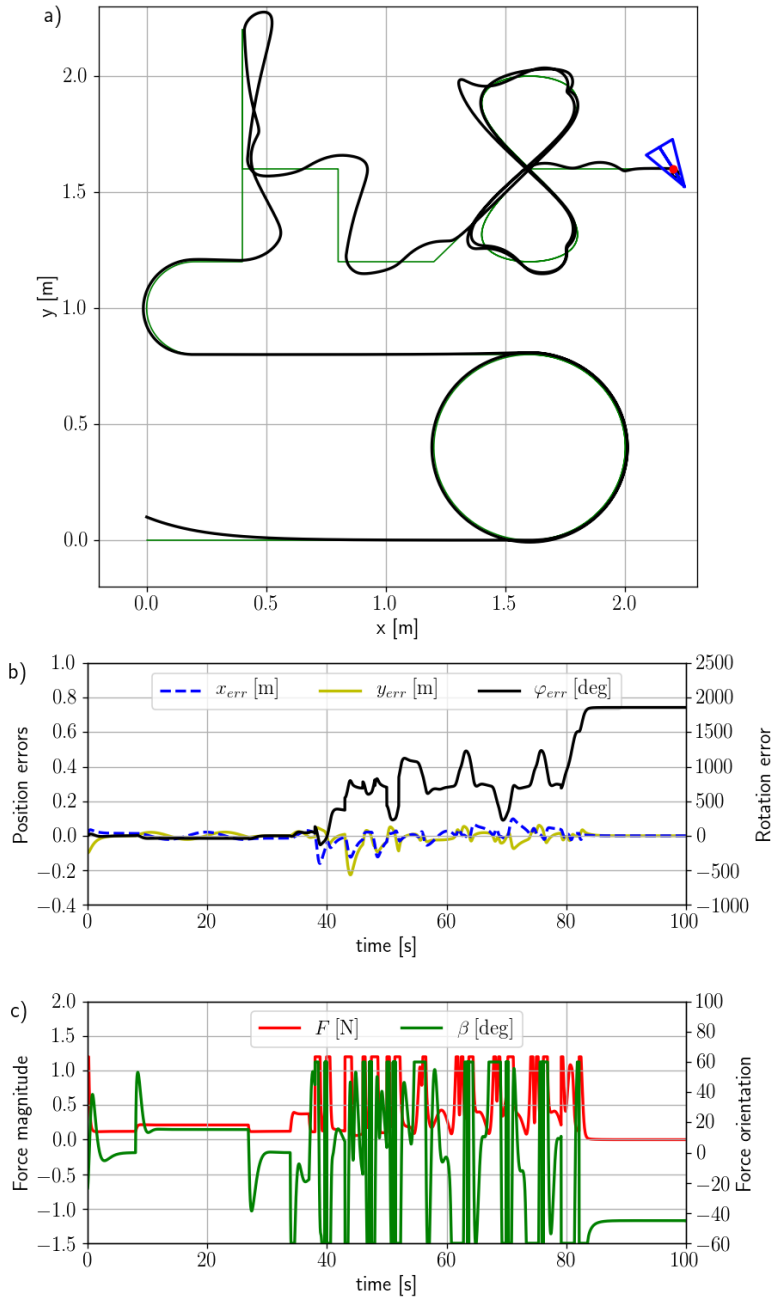


Figure 14: Simulation results of selective control for the hovercraft model (C) with  $k_P = 8.685$ ,  $k_D = 10.0$ : a) desired (green) and achieved (black) trajectories, b) position and rotation errors, c) control signals

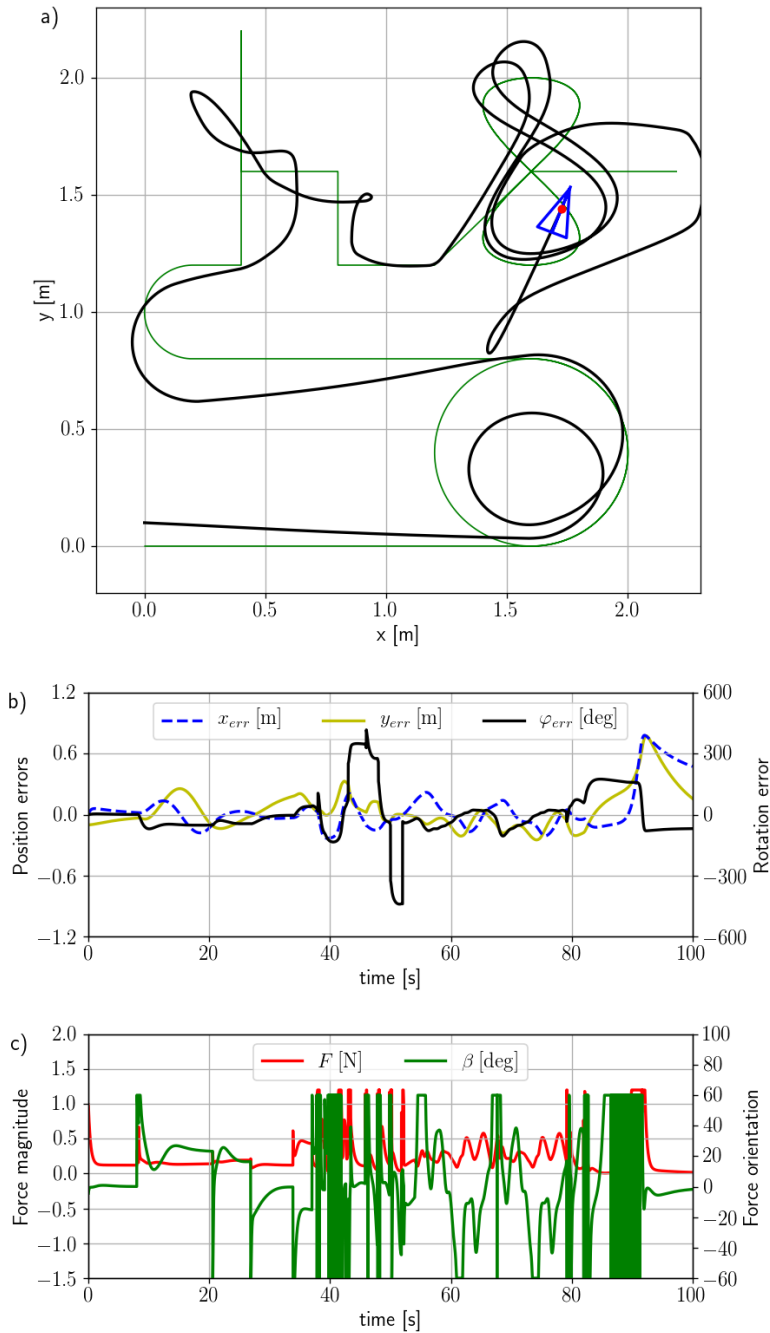


Figure 15: Simulation results of full state control for the hovercraft model (C) with  $k_P = 0.751$ ,  $k_D = 4.939$ ,  $k_{rP} = 1.599$ ,  $k_{rD} = 3.027$ : a) desired (green) and achieved (black) trajectories, b) position and rotation errors, c) control signals

position and rotation stable during whole motion, reducing deviation of angle errors in cost of huge position errors (Figure 15b).

All presented results of optimized selective control (Figures 8, 10, 14) give acceptable good results of position tracking and stable rotation errors with visible 360 degrees jumps. Results of optimized full state control (Figures 9, 11, 15) give stable behavior of position and rotation errors with more visible deviations. Final comparison of simulation results in terms of values of errors is presented in Table 3 (position error from the initial condition was neglected in calculations of  $e_x$  maximum). Values of maximum and root mean square of errors confirm the effect of full state control in relation to selective control – better shape of orientation error together with worse position errors. Total error values proofs, that the Caster Car model with free moving caster has better ability to track presented trajectory than same with blocked casters (for both selective and full state control).

Table 3: Comparison of errors from simulation results for selective and full state methods with all models

Error name	Caster Car blocked (A)		Caster Car free (B)		Hovercraft (C)	
	selective	full	selective	full	selective	full
$e_{x rms}$	0.0302	0.0405	0.0296	0.1007	0.0328	0.2104
$e_{y rms}$	0.0748	0.0507	0.0410	0.1011	0.0344	0.1976
$e_{\varphi rms}$	(4.6205)	1.0013	(4.6472)	0.9500	(16.357)	2.0222
max $e_x$	0.0452	0.3008	0.1170	0.1886	0.0980	0.7813
max $e_y$	0.0344	0.0411	0.1669	0.2362	0.0606	0.7761
max $e_{\varphi}$	(7.8788)	3.1421	(7.5677)	2.6963	(32.434)	7.2852
total	255.08	3173.0	159.93	3037.8	150.395	6459.1

## 6. Conclusions

The presented Caster Car model can be an interesting alternative for mobile platforms that connect dynamic properties of hovercrafts and classical 4-wheeled cars. Its sliding properties come from underactuated dynamics and give a possibility to dynamically change the system’s turning radius up to small values. Various regions of possible positions for three given models presented in the Section 4.2 proofs, that the Caster Car model with free casters has better dynamic accessibility than same with blocked casters, and worse accessibility than the hovercraft model.

The stability of uncontrolled degrees of freedom makes traditional selective control risky for the underactuated Caster Car model. Full state control with computed torque technique, PD feedback, and pseudoinverse gives the ability to suppress unstable behaviors of uncontrolled variables but at the cost of the overall effect. All presented models were successfully controlled during the tracking task with demanding trajectory, including magnitude and direction limitations of input force.

Hovercraft model representation was used to fill the computed torque part of control functions during all simulations – that reduced calculation cost and gives the ability to use the presented algorithm for online calculations of real objects.

The requirement of the full state control method strongly depends on practical realization. Uncontrolled roll and pitch angles of flying machines can result in loss of lift force. Uncontrolled orientation of autonomous vehicles can cause unpleasant feelings for passengers. Control of the orientation is also important in situations of limited space (narrow roads, docking stations, warehouses).

Future research related to the Caster Car model should be focused on path-tracking tasks, online control performance, and mathematical proofs of control loop stability. It can also include a gain scheduling algorithm to switch PD controller parameters depending on the importance of state errors.

### Nomenclature

Variable name	Description
$m$	whole platform mass [kg]
$I_C$	mass moment of inertia respect to the center of mass (point C) [ $\text{kg}\cdot\text{m}^2$ ]
$x(t), y(t)$	platform's center of mass position coordinates [m]
$\varphi(t)$	platform's self rotation angle [rad]
$\vec{F}(t)$	vector of force [N]
$a$	offset of force position wrt. center of mass [m]
$c$	constant drag coefficient for linear motion [ $\text{N}\cdot\text{s}\cdot\text{m}^{-1}$ ]
$c_\varphi$	constant drag coefficient for angular motion [ $\text{N}\cdot\text{m}\cdot\text{s}\cdot\text{rad}^{-1}$ ]
$\beta$	angle of force direction wrt. center line [rad]
$r_F$	radius of front wheel [m]
$I_F$	mass moment of inertia of front wheel [ $\text{kg}\cdot\text{m}^2$ ]
$\alpha(t)$	angle of rotation of the front wheel [rad]
$\omega(t)$	front wheel's angular velocity [ $\text{rad}\cdot\text{s}^{-1}$ ]
$c_\alpha$	front wheel's viscous friction coefficient [ $\text{N}\cdot\text{m}\cdot\text{s}\cdot\text{rad}^{-1}$ ]
$M_{Fn}$	front wheel's driving torque [N·m]
$\gamma_1, \gamma_2$	angles of rotation of left and right caster wheels' yokes [rad]

Variable name	Description
$I_T$	caster yoke mass moment of inertia with respect to its kingpin [ $\text{kg}\cdot\text{m}^2$ ]
$s$	wheel's slip [-]
$Q_F, Q_C$	load of front and caster wheels [N]
$\mu_1, \mu_2, \mu_3, \mu_4, \mu_5$	friction coefficients for wheel/ground contact models [-]
$\mu_6, c_7$	coefficients for caster pivot friction [m], [ $\text{N}\cdot\text{m}\cdot\text{s}\cdot\text{rad}^{-1}$ ]

## References

- [1] A.M. BLOCH: *Nonholonomic mechanics and control*. Springer, 2003.
- [2] S.W. CHESNUTT: Swivel-caster, 1920. US Patent 1,341,630.
- [3] C.O. CHRISTENSEN: Self-steering caster, 1981. US Patent 4,280,246.
- [4] J.R. DOWNING and L.G. WILLIAMS: Cart caster, 1981. US Patent 4,246,677.
- [5] L. ELDÉN: A weighted pseudoinverse, generalized singular values, and constrained least squares problems. *BIT Numerical Mathematics*, **22**(4), (1982), 487–502, DOI: [10.1007/BF01934412](https://doi.org/10.1007/BF01934412)
- [6] I. FANTONI and R. LOZANO: *Non-linear control for underactuated mechanical systems*. Springer Science & Business Media, 2002.
- [7] S. HADDOUT, M. AIT GUENNOUN and Z. CHEN: Engineering example of the constraint forces in non-holonomic mechanical: forklift-truck robot motion. Part I. *Archives of Control Sciences*, **28**(3), (2018), 483–506, DOI: [10.24425/acs.2018.124713](https://doi.org/10.24425/acs.2018.124713)
- [8] R.N. JAZAR: *Vehicle dynamics theory and applications*. Springer, New York; London, 2008.
- [9] S. KORCZAK: Tracking control of an underactuated rigid body with a coupling input force. *Archives of Control Sciences*, **24**(3), (2014), 321–332.
- [10] S. KORCZAK: *Dynamics and stability of underactuated systems with input coupling*. PhD thesis, Warsaw University of Technology, Warsaw, 2016, (in Polish).
- [11] S. KORCZAK: Chaotic behaviors of an underactuated system in the trajectory tracking task. *Archive of Applied Mechanics*, **88**(1-2), (2018), 111–120, DOI: [10.1007/s00419-017-1297-y](https://doi.org/10.1007/s00419-017-1297-y)
- [12] Y. LIU and H. YU: A survey of underactuated mechanical systems. *IET Control Theory Applications*, **7**(7), (2013), DOI: [10.1049/iet-cta.2012.0505](https://doi.org/10.1049/iet-cta.2012.0505)
- [13] M. MITSCHKE: *Dynamik der Kraftfahrzeuge: Antrieb und Bremsung*. Springer, 1995, (in German).
- [14] U. NAGARAJAN, G. KANTOR and R. HOLLIS: The ballbot: An omnidirectional balancing mobile robot. *The International Journal of Robotics Research*, **33**(6), (2014), 917–930, DOI: [10.1177/0278364913509126](https://doi.org/10.1177/0278364913509126)
- [15] D. PAZDERSKI: A robust smooth controller for a unicycle-like robot. *Archives of Control Sciences*, **28**(1), (2018), 155–183, DOI: [10.24425/119081](https://doi.org/10.24425/119081)

- [16] J.M. VERHAEG and D. BROOKES: Vehicle having wheels and castors, 1999. US Patent 5,899,475.
- [17] R.L. WILLIAMS, B.E. CARTER, P. GALLINA and G. ROSATI: Dynamic model with slip for wheeled omnidirectional robots. *IEEE Transactions on Robotics and Automation*, **18**(3), (2002), 285–293, DOI: [10.1109/TRA.2002.1019459](https://doi.org/10.1109/TRA.2002.1019459)
- [18] S. ZEGHLACHE, D. SAIGAA, K. KARA, A. HARRAG and A. BOUGUERRA: Backstepping sliding mode controller improved with fuzzy logic: Application to the quadrotor helicopter. *Archives of Control Sciences*, **22**(3), (2012), 315–342.